Akshay Kale[1]*
Saurin Patel[1]*
Shizhi Qian[2]
Guoqing Hu[3]**
Xiangchun Xuan[1]

[1]Department of Mechanical Engineering, Clemson University, Clemson, SC, USA
[2]Institute of Micro/Nano-technology, Old Dominion University, Norfolk, VA, USA
[3]LNM, Institute of Mechanics, Chinese Academy of Sciences, Beijing, China

Received July 24, 2013
Revised October 11, 2013
Accepted October 20, 2013

Research Article

Joule heating effects on reservoir-based dielectrophoresis

Reservoir-based dielectrophoresis (rDEP) is a recently developed technique that exploits the inherent electric field gradients at a reservoir-microchannel junction to focus, trap, and sort particles. However, the locally amplified electric field at the junction is likely to induce significant Joule heating effects that are not considered in previous studies. This work investigates experimentally and numerically these effects on particle transport and control in rDEP processes in PDMS/PDMS microchips. It is found that Joule heating effects can reduce rDEP focusing considerably and may even disable rDEP trapping. This is caused by the fluid temperature rise at the reservoir-microchannel junction, which significantly increases the local particle velocity due to fluid flow and particle electrophoresis while has a weak impact on the particle velocity due to rDEP. The numerical predictions of particle stream width and electric current, which are the respective indicators of rDEP manipulation and fluid temperature, are demonstrated to both match the experimental measurements with a good accuracy.

Keywords:
Dielectrophoresis / Electroosmosis / Joule heating / Microfluidics / Reservoir
DOI 10.1002/elps.201300343

Additional supporting information may be found in the online version of this article at the publisher's web-site

1 Introduction

Dielectrophoresis (DEP) is an induced particle motion relative to a suspending medium when subjected to a nonuniform electric field [1, 2]. It is a powerful tool that has been extensively used in microfluidic devices for manipulating various particles (both synthetic and biological) [3–6]. The spatial variations in electric field can be generated by fabricating microscale electrodes (i.e. the so-called electrode-based dielectrophoresis) [7–9] or insulators (i.e. the so-called insulator-based dielectrophoresis) [10–13] inside microchannels. We have recently proposed the use of the inherent electric field gradients at a reservoir-microchannel junction to manipulate particles by DEP [14], which we termed reservoir-based dielectrophoresis or rDEP in short [15]. This approach utilizes directly the size difference between a reservoir and a microchannel, and hence eliminates the micro-fabrication of electrical or mechanical parts within the microchannel. It has been demonstrated to focus, trap, and sort both polymer beads and biological cells in our previous works [16, 17].

Joule heating and its effects have been studied experimentally and numerically in electrode- [18–21] and insulator-based [22–25] DEP microchips. It increases the fluid/device temperature and alters the fluid properties, which can cause adverse impacts to both tested samples and microchips [26, 27]. Joule heating may even induce electrothermal flows in the form of two counter-rotating fluid circulations, which have been demonstrated to significantly affect DEP-based particle manipulations [22, 25, 28–33]. For our proposed rDEP technique, the huge amount of fluid in a reservoir, which is normally a few tens microliter as compared to the tens nano-liter fluid inside a typical microchannel, can serve as a heat sink [34, 35] and thus alleviate the Joule heating effects at the reservoir-microchannel junction. However, temperature gradients are still expected to occur at the junction, especially when large electric fields are needed to handle small particles or highly conductive solutions are required to suspend bioparticles. The resulting local nonuniformity in fluid properties can interact with the applied electric field, affecting the fluid, and particle motions in rDEP processes.

This paper presents a combined experimental and numerical study of Joule heating effects on rDEP manipulation

Correspondence: Professor Xiangchun Xuan, Department of Mechanical Engineering, Clemson University, Clemson, SC 29634-0921, USA
E-mail: xcxuan@clemson.edu
Fax: +1-864-656-7299

Abbreviation: rDEP, reservoir-based dielectrophoresis

*These two authors contributed equally to this paper.
**Additional corresponding author: Dr. Guoqing Hu, E-mail: guoqing.hu@imech.ac.cn

Colour Online: See the article online to view Figs. 1–7 in colour.

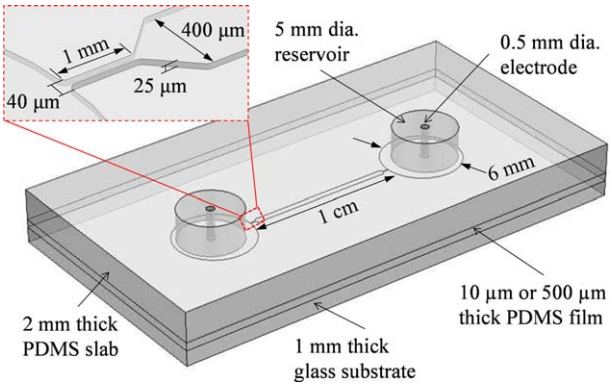

Figure 1. Schematic of the microfluidic chips with geometric specifications indicated.

of particles. The experiment is carried out in PDMS/PDMS microchips with polystyrene particles suspended in a conductive buffer solution. The 3D full-scale numerical model that we developed in an earlier work [31] is employed to predict the coupled electric, temperature, and flow fields under Joule heating effects. The simulated particle trajectories from reservoir to microchannel with and without Joule heating effects are compared with the experimentally observed rDEP focusing and trapping of particles.

2 Materials and methods

2.1 Experimental

To experimentally study the effects of Joule heating on rDEP, we fabricated two microfluidic chips that have identical microchannels for fluid and particle transport but with dissimilar substrates for heat dissipation. The specifications of the two microchips are shown in Fig. 1, which both consist of a 2 mm thick PDMS slab and a 1 mm thick glass slide with a thin layer of PDMS film sandwiched in between. The microchannel is on the bottom surface of the PDMS slab, and is 1 cm long, 25 μm deep, and 400 μm wide in both microchips. It is tapered to a width of 40 μm at the junctions with the two end reservoirs, and the length of the constrictions is 1 mm each. The PDMS film is 10 and 500 μm thick in the two microchips, respectively, through which Joule heating is dissipated at different rates. The thicker the film, the stronger the Joule heating effects are due to the low thermal conductivity of PDMS [25, 36]. It is important to note that the PDMS–PDMS configuration ensures uniform and identical surface properties between the two microchips. The diameter of the reservoirs is 6 mm for the part in the same plane as the microchannel, which is the predefined reservoir size in master fabrication. The rest part of the reservoirs is 5 mm in diameter, determined by the size of the puncher that makes the reservoirs in microchannel fabrication.

The PDMS/PDMS microchips were fabricated using the standard soft lithography technique. The fabrication procedures for the master and the microchannel-containing PDMS slab are identical to those described in our previous work [16] and thus skipped here. To fabricate the 10 μm thick PDMS film, liquid PDMS, formed by mixing the prepolymer and curing agent of PDMS (Sylgard 184 Silicon Elastomer, Dow Corning, Midland, MI) in 10:1 ratio by mass, was spin-coated (Laurell Technologies, North Wales, PA) onto a cleaned glass slide at a speed of 7000 RPM for 50 s [37, 38]. The liquid PDMS layer was then cured at 70°C in a gravity convection oven (13–246–506GA, Fisher Scientific, Fair Lawn, NJ) for 2 h. The 500 μm thick PDMS film was prepared by dispensing a calculated volume of liquid PDMS over a glass slide in a petri dish and curing it in the oven for 2 h. The thicknesses of both PDMS films were measured and confirmed under an inverted microscope (Nikon Eclipse TE2000U, Nikon Instruments, Lewisville, TX). The microchannel-containing PDMS slab and the PDMS film-coated glass slide were bonded together after 1 min plasma treating (PDC-32G, Harrick Scientific, Ossining, PA).

Polystyrene microspheres of 3 μm in diameter (Polyscience, Warrington, PA, USA) were used to study Joule heating effects on rDEP focusing and trapping. They were diluted and re-suspended in 5 mM phosphate buffer with a measured electric conductivity of 1000 μS/cm at room temperature. The electric control of particle transport was achieved by imposing DC-biased AC electric voltages upon two 0.5 mm diameter platinum electrodes that were placed in the two end reservoirs of the microchannel. The voltages were supplied by a function generator (33220A, Agilent Technologies, Santa Clara, CA) in conjunction with a high-voltage amplifier (609E-6, Trek, Medina, NY). The AC voltage frequency was fixed at 1 kHz in all tests. Particle motion at the reservoir-microchannel junction was monitored and recorded using an inverted microscope imaging system (Nikon Eclipse TE2000U, Nikon Instruments). The captured digital images were processed using the Nikon imaging software (NIS-Elements AR 2.30, Nikon Instruments, Lewisville, TX). External pressure-driven flow was eliminated by carefully balancing the liquid heights in the two reservoirs prior to every experiment. A digital multimeter connected in series with the electrical circuit was used to measure the electric current, DC current plus the root-mean-square AC current, through the microchannel.

2.2 Numerical model

The amplified electric field at the constriction in the reservoir-microchannel junction generates a higher local Joule heating of the fluid than in the rest of the microchannel. This leads to heat transfer in the fluid from the constriction into the reservoir and bulk microchannel and in turn the PDMS and glass substrates. Steady state is reached when the heat dissipation rate from the outer surfaces of the microchip to the atmosphere equals the heat generation rate. The resulting temperature distribution affects the electric and flow fields within the microchannel via the temperature-dependent fluid viscosity, electric permittivity, and conductivity. This can cause an

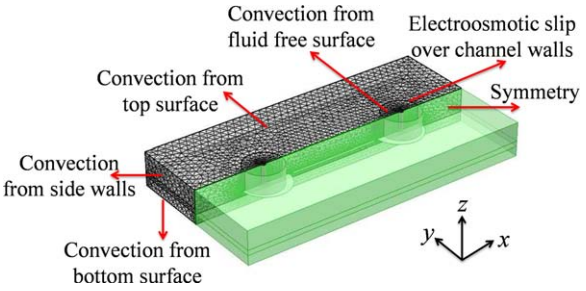

Figure 2. Illustration of the meshed computational domain with boundary conditions indicated on surfaces. The transparent half represents the symmetric nature of the problem.

impact on the particle motion from reservoir to microchannel. Hence the rDEP process is associated with a coupled heat, electricity, and fluid transport, which, as presented below, are governed by the steady-state energy equation, i.e. Eq. (1), electric current conservation equation, i.e. Eq. (2), and Navier–Stokes equations, i.e. Eq. (3), respectively. The mathematical details and assumptions behind these equations are extensively discussed in our previous work [31], and hence not repeated here.

$$\rho C_p \mathbf{u} \bullet \nabla T = k\nabla^2 T + \sigma \mathbf{E}_{DC}^2 \left(1 + r^2\right) \tag{1}$$

$$\nabla \bullet (\sigma \mathbf{E}_{DC}) = 0 \tag{2}$$

$$\nabla \bullet \mathbf{u} = 0 \tag{3a}$$

$$\rho \left(\mathbf{u} \bullet \nabla\right) \mathbf{u} = -\nabla p + \nabla \bullet (\eta \nabla \mathbf{u}) + \left(1 + r^2\right) \left[\nabla \bullet (\varepsilon \mathbf{E}_{DC}) \, \mathbf{E}_{DC} - \frac{1}{2} \mathbf{E}_{DC}^2 \nabla \varepsilon\right] \tag{3b}$$

In the above equations ρ, C_p, k, and T are the mass density, heat capacity, thermal conductivity, and temperature of the fluid or the solid substrate, respectively; $\mathbf{u}$, σ, p, η, and ε are the fluid velocity, electric conductivity, pressure, dynamic viscosity, and electric permittivity, respectively; $\mathbf{E}_{DC}$ is the DC component of the applied DC-biased AC electric fields with r being the AC (root-mean-square values) to DC field ratio or equivalently the AC to DC voltage ratio.

The coupled Eqs. (1)–(3) were solved in one half of the microfluidic chip due to the symmetric nature of the transport phenomena about the center-plane of the microchannel. Figure 2 shows the meshed computational domain along with the surface boundary conditions. The symmetry condition is applied to the surface separating the meshed and transparent (not solved in the model) halves of the microchip. Due to their highly conductive nature for both the electric field and heat flow, the platinum electrodes were treated as holes with iso-potential (at the given DC potentials) and isothermal (at room temperature) conditions. Electroosmotic slip velocity in response to the DC electric field component was imposed on the charged channel walls. Atmospheric pressure condition was applied to the free surfaces of the fluid in the two reservoirs. Natural convection conditions were used for the outer surfaces of the microchip including the fluid free surfaces. The details of the boundary condition settings can be referred to our previous work [31].

To simulate the particle trajectory in the rDEP process, we neglected the inertial and gravity effects and considered only the contributions of fluid flow, $\mathbf{u}$, electrophoresis, $\mathbf{U}_{EP}$, and negative DEP, $\mathbf{U}_{DEP}$, to the particle velocity, $\mathbf{U}_p$, i.e.:

$$\mathbf{U}_p = \mathbf{u} + \mathbf{U}_{EP} + \mathbf{U}_{DEP} \tag{4}$$

$$\mathbf{U}_{EP} = \frac{\varepsilon \zeta_P}{\eta} \mathbf{E}_{DC} \tag{5}$$

$$\mathbf{U}_{DEP} = -\lambda \frac{d^2 \varepsilon}{24\eta} \left(1 + r^2\right) \nabla \mathbf{E}_{DC}^2 \tag{6}$$

In these equations ζ_p and d are the zeta potential and diameter of the particle, and λ is the correction factor that we introduce to account for the particle size effects on DEP [39,40]. Note that the Clausius–Mosotti factor has been set to -0.5 in Eq. (6) because the electric conductivity of 3 μm particles used in our tests, which is 13.3 μS/cm, is much smaller than that of the suspending fluid (1000 μS/cm). This treatment is consistent with that in the paper from Hawkins et al. [41] for the same size of polystyrene particles in DC-biased low-frequency AC electric fields. The former conductivity value was estimated by assuming the surface conductance of polymer particles to be 1 nS as suggested by Ermolina and Morgan [42].

A commercial finite element package, COMSOL 4.3a (www.comsol.com), was used to solve the system of Eqs. (1)–(3) and track the particle motion using the particle velocity from Eq. (4). Nonuniform tetrahedral mesh with a finer mesh in the fluid domain was used. The mesh consists of about two million elements, for which the converged results were confirmed to be mesh independent. The details of the numerical method and model validation are referred to our previous work [31]. The material properties involved in the simulation are presented in the Supporting Information to save space.

3 Results and discussion

Figure 3 compares the rDEP focusing and trapping of 3 μm particles in the microchips with 10 and 500 μm thick PDMS films, respectively, under the application of 20 V DC-biased AC voltages. For each microchip both experimentally obtained streak images (left column) and numerically predicted particle trajectories (right column) are presented, which indicate a close agreement in all tested cases. The numerical results were all extracted at $z = 5$ μm, i.e. 5 μm above the bottom wall of the microchannel (see Fig. 2). This z-slice was selected because particles (with a density of 1.05 g/cm^3) are slightly heavier than the suspending fluid and tend to move close to the bottom channel wall. We, however, note that

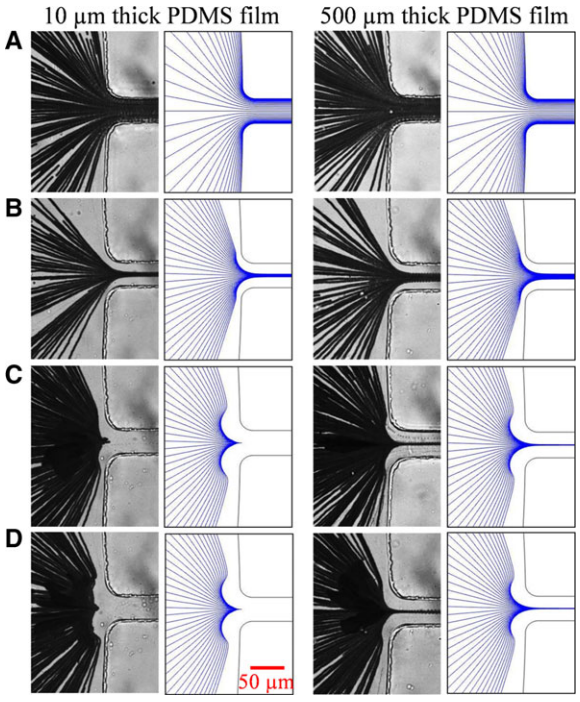

Figure 3. Comparison of rDEP focusing and trapping of 3 μm particles in the microchips with 10 μm and 500 μm thick PDMS films, respectively, under (A) 20 V DC, (B) 20 V DC-200 V AC (i.e. the AC to DC voltage ratio is $r = 10$), (C) 20 V DC-350 V AC (i.e. $r = 17.5$), and (D) 20 V DC-450 V AC (i.e. $r = 22.5$). The left and right columns for each microchip display the experimentally obtained streak images and numerically predicted particle trajectories at the inlet reservoir-microchannel, respectively. The flow direction is from left to right in all cases.

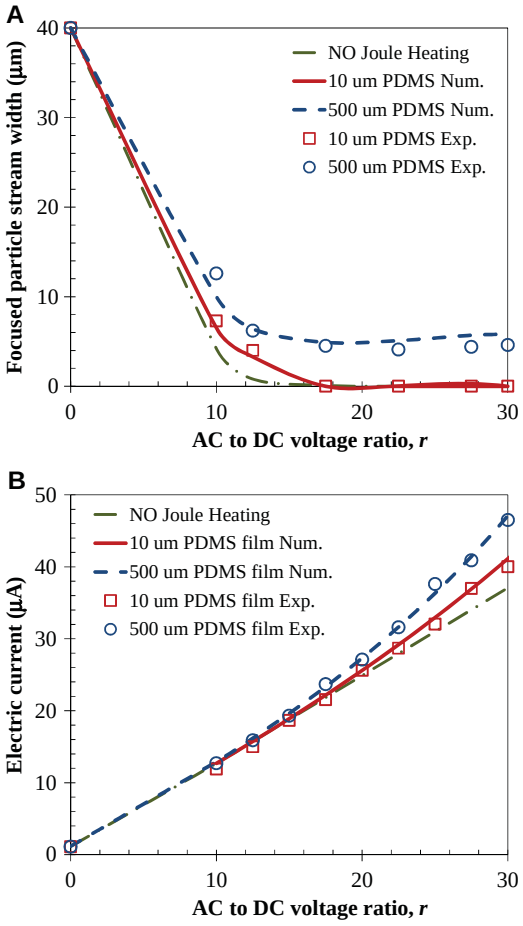

Figure 4. Comparison of the experimentally measured (symbols) and numerically predicted (lines) stream widths of 3 μm particles (A) and electric currents (B) for rDEP focusing and trapping in the microchips with 10 and 500 μm thick PDMS films, respectively. The DC voltage was fixed at 20 V. The dashed-dotted lines in both plots represent the numerical predictions in the absence of Joule heating effects. Note that the vertical spans of the symbols have taken into consideration the experimental errors in measurements.

the predicted particle trajectories do not vary significantly with the z coordinate because the demonstrated rDEP is essentially 2D and takes effects in the x-y plane only. Under a small pure DC voltage in Fig. 3A, i.e. the AC to DC voltage ratio is $r = 0$, particles occupy the entire width of the microchannel in both microchips due to negligible rDEP and Joule heating effects. With the addition of a 200 V AC voltage (i.e. $r = 10$), rDEP increases leading to particle focusing toward the center of the microchannel [14–17] as seen from Fig. 3B. However, the microchip with a 10 μm thick PDMS film achieves an apparently better focusing than that with a 500 μm film. This difference in focusing effectiveness is owed to the unequal temperature build-up in the two microchips because a thicker film imposes a larger thermal resistance to heat transfer. Such Joule heating effects-induced discrepancy in rDEP focusing between the two microchips becomes more obvious with an increasing AC voltage. In Fig. 3C where the AC voltage is 350 V or $r = 17.5$, particles can get trapped by rDEP in the microchip with a 10 μm PDMS film. In contrast, there still appears no particle trapping in the other microchip even under the AC voltage of 450 V (i.e. $r = 22.5$).

A quantitative comparison of the rDEP focusing and trapping of 3 μm particles in the two microchips is shown in Fig. 4A in terms of the focused particle stream width in the microchannel. Both the experimental (symbols) and numerical (lines) results are included in the plot along with the numerical prediction in the absence of Joule heating effects (dashed-dotted lines). Note that the particle stream width simply becomes zero when particles get trapped in front of the reservoir-microchannel junction. The experimentally measured decrease in the focused particle stream width with increasing r is numerically predicted with a good accuracy for the two microchips. Moreover, the observed particle focusing and trapping in both microchips are apparently weaker than those in an ideal Joule heating-free microchip, especially significant for the chip with a thicker PDMS film due to stronger Joule heating effects therein. Interestingly, the particle stream width in the latter does not reduce to zero with increasing r, but begins to increase gradually beyond $r = 20$ as evidenced from both the experiment and modeling in Fig. 4A. This is believed to be the consequence of the induced electrothermal

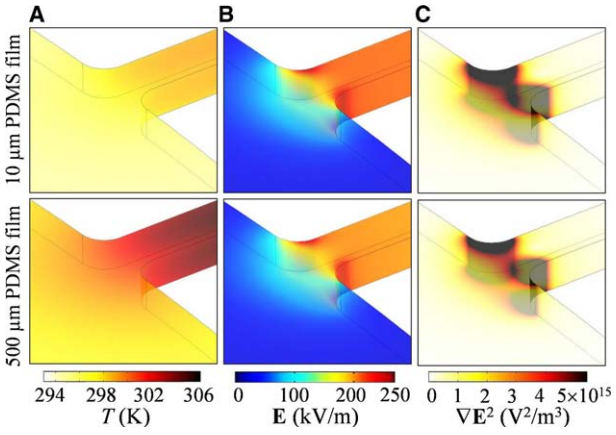

Figure 5. Comparison of the simulated contours of fluid temperature (A), electric field (B), and $\nabla\mathbf{E}^2$ (C) at the reservoir-microchannel junction of the microchips with a 10 μm (top row) and a 500 μm (bottom row) thick PDMS film, respectively. The applied voltage is fixed at 20V DC-350 V AC, i.e. $r = 17.5$, for all cases.

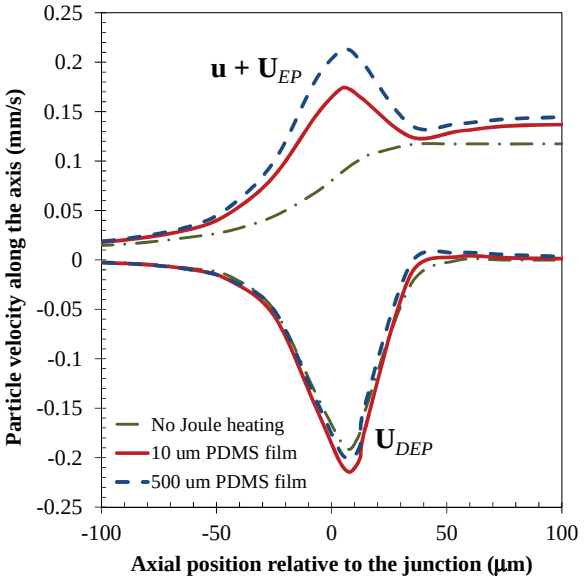

Figure 6. Comparison of the numerically predicted axial particle velocity due to fluid flow and particle electrophoresis, i.e. $\mathbf{u} + \mathbf{U}_{EP}$, with that due to rDEP, i.e. $\mathbf{U}_{DEP}$, of 3 μm particles at the reservoir-microchannel junction of the microchips with a 10 and a 500 μm thick PDMS film, respectively. The entrance of the junction is selected as the origin of the horizontal axis. The applied voltage is fixed at 20 V DC-350 V AC, i.e. $r = 17.5$, for all cases.

flow [22, 23, 29–33] at the reservoir-microchannel junction, which becomes strong enough at large voltages to perturb electroosmotic flow and deteriorate rDEP.

The reduced rDEP focusing and trapping due to Joule heating effects can be viewed from another angle in Fig. 4B, where the experimentally measured (symbols) and numerically predicted (lines) electric currents in the two microchips are illustrated. The microchip with a 500 μm thick PDMS film experiences a higher electric current than that with a 10 μm film. This indicates a greater rise in the average fluid temperature in the former chip. However, the current difference between the two microchips is unnoticeable when the AC to DC voltage ratio, *r*, is less than 15. It is because Joule heating effects are negligible at very small *r*, and the fluid temperature rise is restricted only to the short constrictions at the reservoir-microchannel junctions (which thus has a significant impact on rDEP as explained later) for $r < 15$. This is evidenced from the nearly identical electric currents between the tested microchips and the ideal microchip with no Joule heating (dashed-dotted line) in Fig. 4B. For $r > 15$, the electric current in the microchip with a 500 μm thick PDMS film increases with *r* much faster than that with a 10 μm film as compared to the current in the absence of Joule heating effects. This explains indirectly why rDEP focusing is diminished and rDEP trapping is unachievable in the microchip with a thicker PDMS film at $r > 20$.

To better understand how Joule heating affects rDEP focusing and trapping, we use the numerical model to study the temperature, electric, flow fields, and particle velocity profile at the inlet reservoir-microchannel junction. The case of 20 V DC–350 V AC with the AC to DC voltage ratio, $r = 17.5$, is selected for demonstration because this voltage initiates trapping in the microchip with a 10 μm thick PDMS film but not in the other. Figure 5 shows the contours of the predicted temperature (A), electric field (B), and $\nabla\mathbf{E}^2$ (C) in the fluid domain at the reservoir-microchannel junction. The maximum temperature rise in the microchip with a 500 μm thick PDMS film is about 13°C (bottom row), which almost doubles that with a 10 μm film (top row). However, the fluid temperature in the main body of the microchannel increases by only 2.3°C and 1.3°C in the two microchips, respectively. This explains why the electric currents in both chips are only weakly larger than that in the absence of Joule heating effects; see Fig. 4B. Due to the conservation of electric current, the increase of fluid temperature at the junction causes a slight drop in the local electric field [31]. The greater the fluid temperature rise, the weaker the electric field is at the junction, which can be seen from the electric field contours in Fig. 5B. As a result, the microchip with a thinner PDMS film can provide stronger electric field gradients, i.e. $\nabla\mathbf{E}^2 = \left(1 + r^2\right)\nabla\mathbf{E}_{DC}^2$ in Fig. 5C, which affects particle DEP in Eq. (6) and the electrothermal force in Eq. (3b) (i.e. the square bracketed term).

Figure 6 shows the comparison of the numerically predicted axial particle velocity due to fluid flow and particle electrophoresis, i.e. $\mathbf{u} + \mathbf{U}_{EP}$, against that due to rDEP, i.e. $\mathbf{U}_{DEP}$, of 3 μm particles at the reservoir-microchannel junction in the two microchips. With reference to $\mathbf{u} + \mathbf{U}_{EP}$ in an ideal Joule heating-free microchip (dashed-dotted line), we find that Joule heating effects increase the particle velocity due to fluid flow and particle electrophoresis. This indicates that the decrease in electric field (see Fig. 4B) is counter-balanced by the increase in the fluid property ratio, ε/η (see Eqs. (5) and (6)) with the rise of fluid temperature. Interestingly, there appears a peak in the curve of $\mathbf{u} + \mathbf{U}_{EP}$ at the junction in each of the two tested microchips, which is, however, absent when Joule heating effects are ignored. This phenomenon is

attributed to the Joule heating-induced electrothermal force in Eq. (3b), i.e. the square bracketed term on the right-hand-side. The resulting electrothermal flow, which is confined to the reservoir-microchannel junction due to the local temperature gradients, is superimposed onto fluid electroosmosis and particle electrophoresis, leading to the observed variation of $\mathbf{u} + \mathbf{U}_{EP}$ in Fig. 6. In contrast, the dielectrophoretic particle velocity, $\mathbf{U}_{DEP}$, is much less sensitive to Joule heating effects. As demonstrated in Fig. 6, the microchip with a 10 μm thick PDMS film offers an inconsiderably stronger $\mathbf{U}_{DEP}$ than that with a 500 μm film at the junction. This is because the higher fluid property ratio, ε/η, in the latter due to a greater temperature rise (see Fig. 5A) is insufficient to compensate for its smaller gradients of electric field squared, i.e. $\nabla\mathbf{E}^2$ in Fig. 5C, along the channel centerline. However, $\mathbf{U}_{DEP}$ in both microchips still has a slightly larger magnitude than that in the ideal Joule heating-free chip.

The ultimate effects of Joule heating on rDEP manipulation can be evaluated in terms of a particle trapping number, τ, which is defined as the ratio of the axial particle velocity due to rDEP with respect to the axial particle velocity due to fluid flow and particle electrophoresis, i.e. $\tau = (\mathbf{U}_{DEP})_{\text{axis}}/(\mathbf{u} + \mathbf{U}_{EP})_{\text{axis}}$. Figure 7A shows the axial profiles of this dimensionless number in the two tested microchips and the ideal Joule heating-free chip. Note that rDEP trapping occurs in the place where $\tau \geq 1$, which is depicted in the plot as a dotted line. The local enhancement of $\mathbf{u} + \mathbf{U}_{EP}$ at the reservoir-microchannel junction due to electrothermal flow (Fig. 6) significantly reduces the particle trapping number. Such an influence from Joule heating effects is strong enough to reduce the trapping number below 1 for the microchip with a 500 μm thick PDMS film. This explains why particles are not trapped by rDEP in this microchip, which is consistent with the experimental observation in Fig. 3C. We also compare the peak trapping numbers, which appears at or near the junction, in the microchips with and without Joule heating effects at various AC to DC (fixed at 20 V) voltage ratios. As seen from Fig. 7B, the peak trapping number in the microchip with a 500 μm thick PDMS film never exceeds 1 (dotted line) and even reduces with the AC to DC voltage ratio for $r > 20$. This agrees with the trend of the experimentally measured particle stream width in Fig. 4A. In contrast, the peak trapping number in the microchip with a 10 μm film reaches 1 at about $r = 14$, and continues increasing slowly at higher r. It is, however, smaller than that in a Joule heating-free microchip, especially significant at large values of r.

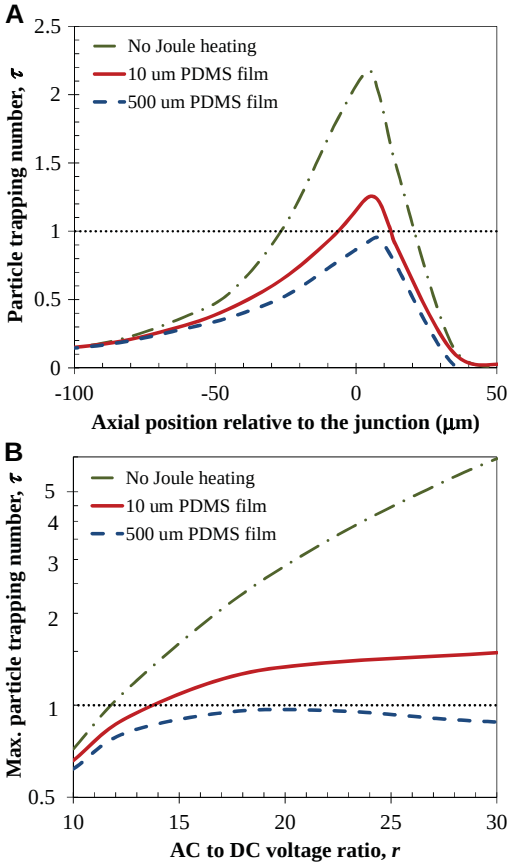

Figure 7. Comparison of the numerically predicted trapping number, $\tau = (\mathbf{U}_{DEP})_{\text{axis}}/(\mathbf{u} + \mathbf{U}_{EP})_{\text{axis}}$, for 3 μm particles at the reservoir-microchannel junction of the microchips with a 10 μm and a 500 μm thick PDMS film, respectively. (A) Shows the axial profiles of the trapping number at 20 V DC-350 V AC, i.e. $r = 17.5$, where the entrance of the junction is selected as the origin of the horizontal axis; (B) shows the peak trapping number as a function of the AC to DC (fixed at 20 V) voltage ratio. The dotted lines indicate the threshold at which rDEP trapping occurs.

4 Concluding remarks

We have conducted a fundamental study of the effects of Joule heating on particle transport and control in rDEP. The experimental observations and numerical predictions have been found to agree closely. By comparing the particle stream widths in two identical microchannels with unequal heat dissipation rates, we have demonstrated that Joule heating can considerably reduce rDEP focusing and may even disable rDEP trapping. These changes are further confirmed by reference to the rDEP performance in an ideal Joule heating-free microchip. They are caused by the fluid temperature rise, which, as indicated by the increase in electric current, weakly reduces the electric field at the reservoir-microchannel junction while strongly increasing the fluid property ratio, ε/η. This in turn increases significantly the particle velocity due to fluid flow and particle electrophoresis at the junction, but has an insignificant impact on the particle velocity due to rDEP. Such influences have also been presented in terms of a dimensionless particle trapping number, which is useful for determining the conditions under which particle trapping can take place in insulator-based dielectrophoresis microchips.

This work is partially supported by NSF under grant CBET-0853873 (Xuan), NRF of Korea under grant 2011–0014246 (Qian), and by NSFC under grant 11272321 (Hu). The Open

Fund support from LNM (Xuan and Hu) is also gratefully acknowledged.

The authors have declared no conflict of interest.

5 References

[1] Pohl, H. A., *Dielectrophoresis: The Behavior of Neutral Matter in Non-uniform Electric Fields*, Cambridge University Press, Cambridge 1978.

[2] Morgan, H., Green, N. G., AC *Electrokinetics—Colloids and Nanoparticles*, Research Studies Press Limited, Baldock, Hertfordshire 2001.

[3] Lapizco-Encinas, B. H., Rito-Palomares, M., *Electrophoresis* 2007, *28*, 4521–4538.

[4] Pethig, R., *Biomicrofluidics* 2010, *4*, 022811.

[5] Jesus-Perez, N. M., Lapizco-Encinas, B. H., *Electrophoresis* 2011, *32*, 2331–2357.

[6] Cetin, B., Li, D., *Electrophoresis* 2011, *32*, 2420–2427.

[7] Gascoyne, P. R. C., Vykoukal, J., *Electrophoresis* 2002, *23*, 1973–1983.

[8] Hughes, M. P., *Electrophoresis* 2002, *23*, 2569–2582.

[9] Gagnon, Z. R., *Electrophoresis* 2011, *32*, 2466–2487.

[10] Chou, C. F., Zenhausern, F., *IEEE Eng. Med. Biology Mag.* 2003, *22*, 62–67

[11] Cummings, E. B., *IEEE Eng. Med. Biology Mag.* 2003, *22*, 75–84.

[12] Srivastava, S. K., Gencoglu, A., Minerick, A. R., *Anal. Bioanal. Chem.* 2010, *399*, 301–321.

[13] Regtmeier, J., Eichhorn, R., Viefhues, M., Bogunovic, L., Anselmetti, D., *Electrophoresis* 2011, *32*, 2253–2273.

[14] Zhu, J., Hu, G., Xuan, X., *Electrophoresis* 2012, *33*, 916–922.

[15] Xuan, X., *Reservoir-based dielectrophoresis*, AES Electrophoresis Society, Application Foci on Dielectrophoresis, 2012, http://www.aesociety.org/areas/ rdep.php.

[16] Patel, S., Showers, D., Vedantam, P., Tzeng, T. J., Qian, S., Xuan, X., *Biomicrofluidics* 2012, *6*, 034102.

[17] Patel, S., Qian, S., Xuan, X., *Electrophoresis* 2013, *34*, 961–968.

[18] Ramos, A., Morgan, H., Green, N. G., Castellanos, A., *J. Phys. D* 1998, *31*, 2338–2353.

[19] Castellanos, A., Ramos, A., Gonzalez, A., Green, N. G., Morgan, H., *J. Phys. D* 2003, *36*, 2584–2597.

[20] Grom, F., Kentsch, J., Müller, T., Schnelle, T., Stelzle, M., *Electrophoresis* 2006, *27*, 1386–1393.

[21] Burg, B. R., Bianco, V., Schneider, J., Poulikakos, D., *J. Appl. Phys.* 2010, *107*, 124308.

[22] Hawkins, B. G., Kirby, B. J., *Electrophoresis* 2010, *31*, 3622–3633

[23] Sridharan, S., Zhu, J., Hu, G., Xuan, X., *Electrophoresis* 2011, *32*, 2274–2281

[24] Braff, W. A., Pignier, A., Buie, C. R., *Lab Chip* 2012, *12*, 1327–1331.

[25] Zellner, P., Agah, M., *Electrophoresis* 2012, *33*, 2498–2507.

[26] Xuan, X., *Electrophoresis* 2008, *29*, 33–43.

[27] Cetin, B., Li, D., *Electrophoresis* 2008, *29*, 994–1005.

[28] Gao, J., Sin, M. L., Liu, T., Gau, V., Liao, J. C., Wong, P. K., *Lab Chip* 2011, *11*, 1770–1775.

[29] Zhu, J., Sridharan, S., Hu, G., Xuan, X., *J. Micromech. Microeng.* 2012, *22*, 075011.

[30] Chaurey, V., Polanco, C., Chou, C. F., Swami, N. S., *Biomicrofluidics* 2012, *6*, 012806.

[31] Kale, A., Patel, S., Hu, G., Xuan, X., *Electrophoresis* 2013, *34*, 674–683.

[32] Chaurey, V., Rohani, A., Su, Y. H., Liao, K. T., Chou, C. F., Swami, N. S., *Electrophoresis* 2013, *34*, 1097–1104.

[33] Gallo-Villanueva, R. C., Sano, M. B., Lapizco-Encinas, B. H., Davalos, R. V., *Electrophoresis* 2014, *35*, 352–361

[34] Xuan, X., Xu, B., Sinton, D., Li, D., *Lap Chip* 2004, *4*, 230–236.

[35] Tang, G., Yan, D., Yang, C., Gong, H., Chai, J. C., Lam, Y. C., *Electrophoresis* 2006, *27*, 628–639.

[36] Erickson, D., Sinton, D., Li, D., *Lab Chip* 2003, *3*, 141–149

[37] Koschwanez, J. H., Carlson, R. H., Meldrum, D. R., *PLoS One* 2009, *4*, e4572.

[38] Zhang, W. Y., Ferguson, Gregory S. Tatic-Lucic, S., 17th IEEE International Conference on Micro Electro Mechanical Systems, 2004, pp. 741–744.

[39] Kang, K., Kang, Y., Xuan, X., Li, D., *Electrophoresis* 2006, *27*, 694–702.

[40] Zhu, J., Xuan, X., *Electrophoresis* 2009, *30*, 2668–2675.

[41] Hawkins, B. G., Smith, A. E., Syed, Y. A., Kirby, B. J., *Anal. Chem.* 2007, *79*, 7291–7300.

[42] Ermolina, I., Morgan, H., *J. Colloid Interface. Sci.* 2005, *285*, 419–428.

